Creating 3D objects with integrated electronics via multiphoton fabrication *in vitro* and *in vivo*

Sara J. Baldock, Punarja Kevin,† Garry R. Harper,† Rebecca Griffin,† Hussein H. Genedy, M. James Fong, Zhiyi Zhao, Zijian Zhang, Yaochun Shen, Hungyen Lin, Catherine Au, Jack R. Martin, Mark D. Ashton, Mathew J. Haskew, Beverly Stewart, Olga Efremova, Reza N. Esfahani, Hedley Emsley, John B. Appleby, David Cheneler, Damian M. Cummings, Alexandre Benedetto and John G. Hardy**

Dr. S. J. Baldock, Dr. P. Kevin, Dr. G. R. Harper, R. Griffin, H. H. Genedy, Dr. M. J. Fong, Dr. M. D. Ashton, Dr. M. J. Haskew, Dr. J. G. Hardy.
Department of Chemistry, Lancaster University, Lancaster, Lancashire, LA1 4YB, UK.
E-mail: j.g.hardy@lancaster.ac.uk

Dr. Z. Zhao, Dr. Z. Zhang, Prof. Y. Shen.
Department of Electrical Engineering and Electronics, University of Liverpool, Liverpool, L69 3GJ, UK.

Dr. H. Lin, Dr. D. Cheneler.
Department of Engineering, Lancaster University, Lancaster, Lancashire, LA1 4YW, UK.

R. Griffin, J. R. Martin, C. Au, Dr. A. Benedetto.
Division of Biomedical and Life Sciences, Lancaster University, Lancaster, Lancashire, LA1 4YQ, UK.
E-mail: a.benedetto@lancaster.ac.uk

Dr. A. Benedetto.
Centre for Ageing Research, Lancaster University, Lancaster, Lancashire, LA1 4YQ, UK.

Dr. B. Stewart.
School of Chemistry and Biosciences, University of Bradford, Bradford, West Yorkshire, BD7 1DP, UK.

Dr. O. Efremova.

NeuDrive Ltd., Daresbury Laboratory, Sci-Tech, Keckwick Lane, Daresbury, Warrington, Cheshire, WA4 4AD, UK.

Dr. R. N. Esfahani
The Manufacturing Technology Centre, Ansty Business Park, Coventry, West Midlands, CV7 9JU, England, UK.

Prof. H. Emsley.
Lancashire Teaching Hospitals NHS Trust, Royal Preston Hospital, Sharoe Green Lane, Preston, Lancashire, PR2 9HT, UK.

Dr J. B. Appleby, Prof. H. Emsley.
Lancaster Medical School, Health Innovation One, Sir John Fisher Drive, Lancaster University, Lancaster, Lancashire, LA1 4AT, UK.

Dr. D. M. Cummings.
Department of Neuroscience, Physiology and Pharmacology, University College London, London, WC1E 6BT, UK.

Dr D. Chelener, Dr. J. G. Hardy.
Materials Science Institute, Lancaster University, Lancaster, Lancashire, LA1 4YB, UK.

† These authors contributed equally.
* Corresponding authors: a.benedetto@lancaster.ac.uk and j.g.hardy@lancaster.ac.uk

Keywords: additive manufacturing, bioelectronics, conducting polymers, integrated electronics, neural electrodes.

3D objects with integrated electronics were produced using an additive manufacturing approach relying on multiphoton fabrication (direct laser writing, DLW). Conducting polymer-based structures (with micrometer-millimeter scale features) were printed within exemplar matrices, including an elastomer (polydimethylsiloxane, PDMS) widely investigated for biomedical applications. The fidelity of the printing process in PDMS was assessed by optical coherence tomography, and the conducting polymer structures were

demonstrated to be capable of stimulating mouse brain tissue *in vitro*. Furthermore, the applicability of the approach to printing structures *in vivo* was demonstrated in live nematodes (*Caenorhabditis elegans*). These results highlight the potential for such additive manufacturing approaches to produce next-generation advanced material technologies, notably integrated electronics for technical and medical applications (e.g., human-computer interfaces).

1.0. Introduction.

Advances in the manufacturing and miniaturization of electronics and components thereof (computers, microprocessors, transistors, etc.) has revolutionised our lives with the ubiquity of electronic devices in our daily lives, and underpins the economic success of countries across the world.[1] Electronic technologies employ conductors/semiconductors to fulfil specific roles within manufactured devices, and for a variety of reasons organic conductors and semiconductors (e.g., derivatives of carbon nanotubes, graphene, conjugated polymers, etc.) are playing an increasingly important role in these devices (e.g., in flexible/printable electronics, electronic interfaces for the body, etc.).[2-19]

Integrated circuits used in electronics worldwide (e.g., for applications including, but not limited to, amplifiers, logic units, sensors, etc.) are typically mass produced in a layer-by-layer approach.[1] The manufacture of 3D objects with integrated electronics has become an area of intense research interest with a view to the development of flexible electronics.[3,7,11,20,21 22]

There are a number of FDA-approved medical devices capable of electrical stimulation within the body, including cardiac pacemakers, bionic eyes, bionic ears and electrodes for deep brain stimulation; all of which are designed for long-term implantation (via a technically challenging surgical procedure).[3] Conducting polymers (e.g., polyaniline, polypyrrole (PPY), poly(3,4-ethylenedioxythiophene) PEDOT) can electrically stimulating cells *in vitro*, and have proven well-tolerated when implanted into small mammals (e.g., mice, rats and rabbits). Their immunogenicity profile is comparable to FDA-approved non-conductive polymers such as poly(lactic-co-glycolic acid) (PLGA), supporting their safety *in vivo*; these preclinical studies suggest that conducting polymer-based biomaterials are promising for eventual clinical translation.[23]

Furthermore, the tunable properties of conducting polymers (CPs, e.g., derivatives of polyaniline, polypyrrole, polythiophene) make them versatile components of electronic devices.[24] Various methods can be used for CP preparation (including solution phase synthesis, solid phase synthesis, electropolymerization, vapor deposition or photopolymerization), offering opportunities for inclusion in most standard electronic device manufacturing processes.[25,26]

There are a number of approaches to prepare flexible bioelectronics,[3,11,27-30] often involving layer-by-layer processing,[31] however, novel photochemical techniques are under development (e.g., for ion conductive hydrogels).[32] Such approaches are effective routes to functional electronic devices, the ability to prepare electronics with de-novo designed architectures via

printing is appealing for technical and medical applications. It is possible to employ additive manufacturing (AM) techniques to produce components for electronic applications,[33,34] for example printing CP-based materials using various methods, including: extrusion, inkjet printing, photopolymerization, rotary printing, screen printing, etc..[35]

Multiphoton fabrication is an AM approach that potentially allows the manufacture of bespoke architectures with features on various length scales (i.e., nm/μm to mm scale) either free standing (e.g., on glass) or embedded within a matrix of another substance (e.g., in Nafion® sheets), useful for production of integrated circuits[36,37] within the complex geometry of 3D printed parts and addressing limitations in applications where a high level of customization is required.[38-40] Herein, the concept was applied to printing conducting polymer (PPY)-based structures [41] within insulators (e.g., PDMS and shape memory polymers [SMPs][42-45]) *in vitro* and *in vivo* in transparent nematode worms (*C. elegans*). The functionality of the structures for biomedical applications was exemplified by using the conducting polymer-based structures embedded in PDMS to stimulate electrical activity in nerve tissue (an *in vitro* brain tissue paradigm). Such 3D printed electronics may facilitate fundamental studies (*in vitro* and *in vivo*) of the nervous system and its connectivity (e.g., enabling precise, long-term and continuous monitoring of patients over their lifetimes); or indeed the production of bioelectronic devices capable of continuous monitoring and modulation of neural activity. A particularly exciting aspect of the 3D printed electrodes is the potential to tailor electrode array designs specific to patients and their needs. Integration with artificial intelligence and machine learning approaches [46-49] for the development and operation of smart neuromodulation systems and/or human computer interfaces (potentially also useful for the gaming and virtual reality industries), would further support the transition from Industry 4.0 (technology-driven manufacturing) to Industry 5.0 (human-centric design and resilient/sustainable bespoke manufacturing).[50-52]

2.0. Results and Discussion.

2.1. Additive manufacturing of conducting polymer-based electronics integrated in 3D objects *in vitro*.

A variety of computational approaches (with different length and time scales) can be applied to study materials and facilitate the development/production of advanced functional materials for a broad spectrum of technical and medical applications.[53,54] The integration of computational materials engineering approaches in workflows applies the Materials Genome Initiative concept for accelerating the discovery, manufacture and deployment of advanced

materials which underpin millions of jobs worldwide in an area of high economic growth.[55,56] We envision *in silico* approaches supporting the additive manufacturing of advanced functional materials for bioelectronic applications (e.g., in ink formulation, additive manufacturing process optimization, etc.). Understanding the cytocompatibility/biocompatibility of materials is important when contemplating their potential for various applications and their end-of-life.[57-59] *In silico* toxicity screening has been developed to predict negative outcomes in various organisms (mammals, humans, etc.) and in the environment if exposed to molecules (e.g., those being developed for agriculture/healthcare markets);[60-66] the large datasets offer a more reliable/robust method of assessing toxicity than individual measures such as the median lethal dose (LD50)[67] which are prone to variations between testing factors (administration method, environmental factors, genetics, species, etc.),[68] and moreover, conform to the most important principles of processes involving animals in ethically sound research and development (i.e., replacement, reduction and refinement, the 3Rs).[61,69-71] We have previously employed Derek Nexus and Sarah Nexus (Derek Nexus is an expert rule-based system to identify structural alerts for several endpoints and Sarah Nexus is a statistical-based model focused on mutagenicity only) to assess the biocompatibility of biomaterials,[72-74] including PDMS,[75] which is popular in biomedical applications (e.g., coatings of cochlear implants) due to its flexibility and transparency.[7,76-78] However, PDMS contains ether/organosilicon bonds which may be hepatotoxic/nephrotoxic,[79-81] it may degrade [82,83] and its surface chemistry may need to be tuned to minimize biofouling;[84-86] pyrrole (acknowledged in supplier's safety data sheets [SDSs], which are of variable quality, to display a degree of toxicity, with significant variation in LD50 between species and mode of administration), the photoinitiator (Irgacure D2959; SDSs indicating it to be somewhat toxic), and PPY (non-hazardous in supplier's SDSs), which were predicted to be non-sensitizers of skin, and non-mutagenic.[73,87] Here we screen the other components utilized in the printing of PPY-based structures within PDMS (employing ink formulations composed of mixtures of: the monomer pyrrole, PY; the photoinitiator (Irgacure D2959), dopant (camphorsulfonic acid, CSA; SDSs indicating it to be corrosive and toxic), and a combination of polyethyleneglycol (PEG, 10 kDa; SDSs indicating it to be non-hazardous) and polyethyleneglycoldimethyacrylate (PEGDMA, 2 kDa; SDSs variable, often indicated to be an eye irritant, skin sensitizer and toxic), depicted in **Figure 1**). *In silico* toxicity screening studies of the ink components (CSA, and PEG, **Table S1**) using Derek Nexus (Derek Nexus: 6.0.1, Nexus: 2.2.2) predicted them to be non-sensitizers of skin, and *in silico* mutagenicity screening studies using Sarah Nexus (Sarah Nexus: 3.0.0, Sarah

Model: 2.0) predicted them to be non-mutagenic; by contrast, PEGDMA is predicted to plausibly cause chromosome damage, cause irritation of eyes/skin, be a sensitizer of skin (albeit non-mutagenic). In the case of the PPY electronics integrated in PDMS films, it is possible to contemplate their use as conformable bioelectrodes *in vivo* (however, the potential for slow degradation of PDMS[82,83] means they may need to be removed after some time *in vivo*, pending lifetime assessments), or indeed as bioelectrodes for *in vitro* studies.

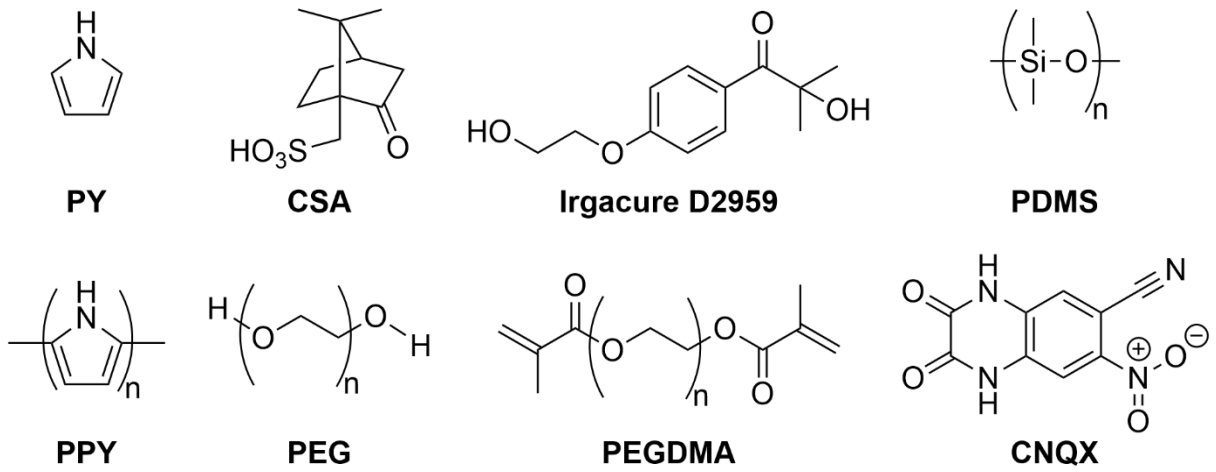

Figure 1. Structures of chemicals used for fabrication of CSA-doped PPY in/on PDMS films and *in vitro* validation of function as electrodes capable of stimulating brain tissue.

Thin films of PDMS were prepared by spin coating (**Table S2**) and swollen with ink formulations composed of mixtures of PY, Irgacure D2959, CSA, PEG and PEGDMA. A commercially available multiphoton fabrication apparatus (Nanoscribe® Photonic Professional GT 700) was used to print structures based on computer aided design (CAD) models via the polymerization of PY (yielding PPY), enabling the fabrication of conductive structures within and on the surface of the PDMS that would facilitate connection to other devices/objects. Once the multiphoton fabrication process was complete, the substrate was washed with ethanol/water to remove traces of low molecular weight contaminants and dried, yielding prototype electrodes with interconnecting wires based on printed conducting polymer structures (CSA-doped PPY) with feature sizes from micrometer to millimeter scale integrated in PDMS.

The darkly colored printed structures were visible by eye within the transparent PDMS matrices (an optical microscope image is shown in **Figure 2A**), the conductivity of which was measured using a probe station and observed to be 3.9 ± 0.3 S/m (**Figure 2B**). SEM of PPY/PDMS structures (**Figure 2C**) shows the printed PPY structures emerge from the PDMS

matrices, and corresponding EDX spectroscopy of the Kα emission of C of the PPY/PDMS structures (**Figures 2D**) show correspondingly enhanced carbon content (red) in the printed PPY structures that emerge from the PDMS matrices (mostly black). FTIR spectroscopy confirmed the printed structures were PPY (**Figure 2E**); the PDMS matrices had characteristic peaks at 789-796 cm^{-1} ($-CH_3$ rocking and Si-C stretching in $Si-CH_3$), 1020-1074 cm^{-1} (Si-O-Si stretching), 1260–1259 cm^{-1} (CH_3 deformation in $Si-CH_3$), and the samples with PPY structures in/on the PDMS have additional peaks characteristic of the PPY (C–C stretching at 1560 cm^{-1}, C–N stretching at 1435 cm^{-1}, =C–H in-plane vibration at 1315 cm^{-1}, C–H or C–N in-plane deformations at 1260 and 1280 cm^{-1}, respectively).

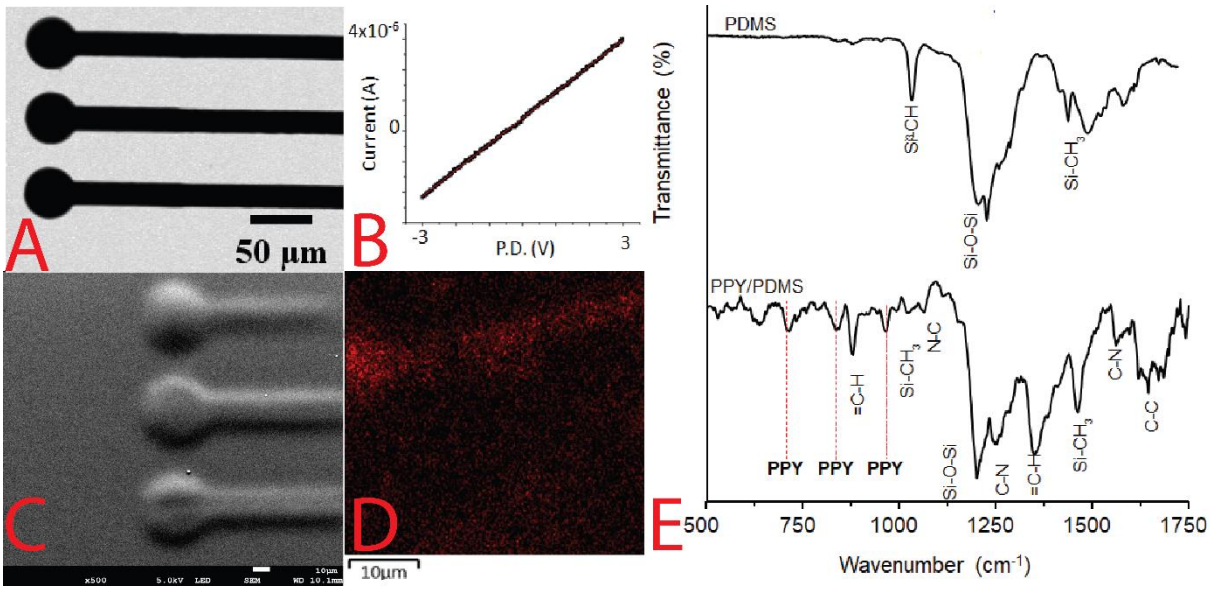

Figure 2. A) Optical microscope image of an exemplar PPY/PDMS structure (scale bar represents 50 µm). B) FTIR spectra of PDMS, PPY/PDMS structures. C) SEM image of an exemplar PPY/PDMS structure (scale bar represents 10 µm). D) EDX image of an exemplar PPY/PDMS structure, where the intensity of Kα emission of C (red) is mapped relative to the background PDMS (black); the scale bar represents 10 µm. E) FTIR spectra of PDMS and PPY/PDMS.

The fidelity of the printing process was assessed by comparison of the CAD files of the designed structures and optical coherence tomography (OCT, for setup see **Figure S1**) of the structures actually printed, an example of which for PPY/PDMS structures is depicted in **Figure 3**. For PPY/PDMS structures we observed the fidelity of the printing process in the X-Y dimensions to be ca. 100 ± 7%, however, in the Z dimension it was much more variable, assessed to be ca. 25% for thick structures (desired thickness of 65 µm), whereas ca. 540% for

thinner structures (desired thickness of 5 µm), see also **Figures S2-S5**. The variations in actual vs. desired structures are caused by heating of the inks/PDMS matrices during the printing process and absorption of light as the monomers polymerize yielding darkly coloured conjugated polymers and should be possible to further optimize. Future optimization of the printing process in an application-/technology-specific fashion will enable the integration of plastic electronics solutions (such as OTFTs and memristors that would allow recording of the action potentials as well as stimulation), printed antennas and batteries for powering and data transmission, which may enable continuous monitoring and modulation.[1]

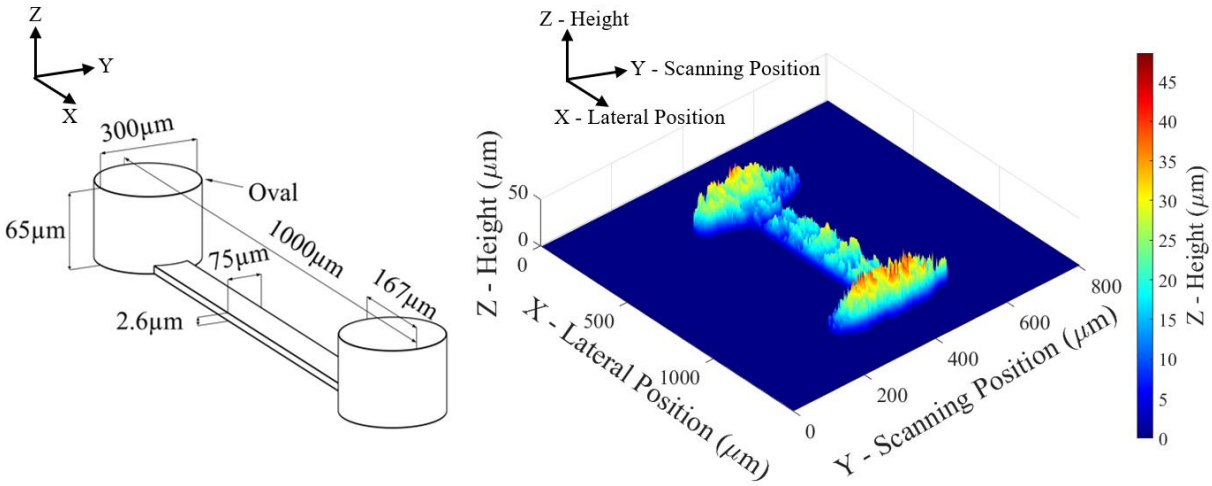

Figure 3. 3D rendering of PPY/PDMS polymer electrode structures. Left) Example CAD structure. Right) Actual structure produced as observed by OCT.

Field stimulation experiments focusing on a single polymer electrode and its operational environment were simulated using a EM field solver in ANSYS Electronics Desktop 2020 R2 using Maxwell 3D with Electric Transient solution type (see **Figure 4**). Here, the tissue was simplified to be a homogeneous material with a conductivity of 0.33 S/m, which is similar to that of mouse brain tissue.[88] These simulations show how the electric field and current density is expected to evolve as the stimulation is applied if there were no cellular activity within the tissue and can be used to optimize experimentation. Simulations show that electric fields established initially between the polymer electrode and glass field electrode upon stimulation result in a flow of charge towards the glass field electrode, as expected. This acts to reduce the electric field gradient within the tissue in accordance with Gauss' law reaching a steady state

(under constant voltage excitation) within ca. 5 µs.

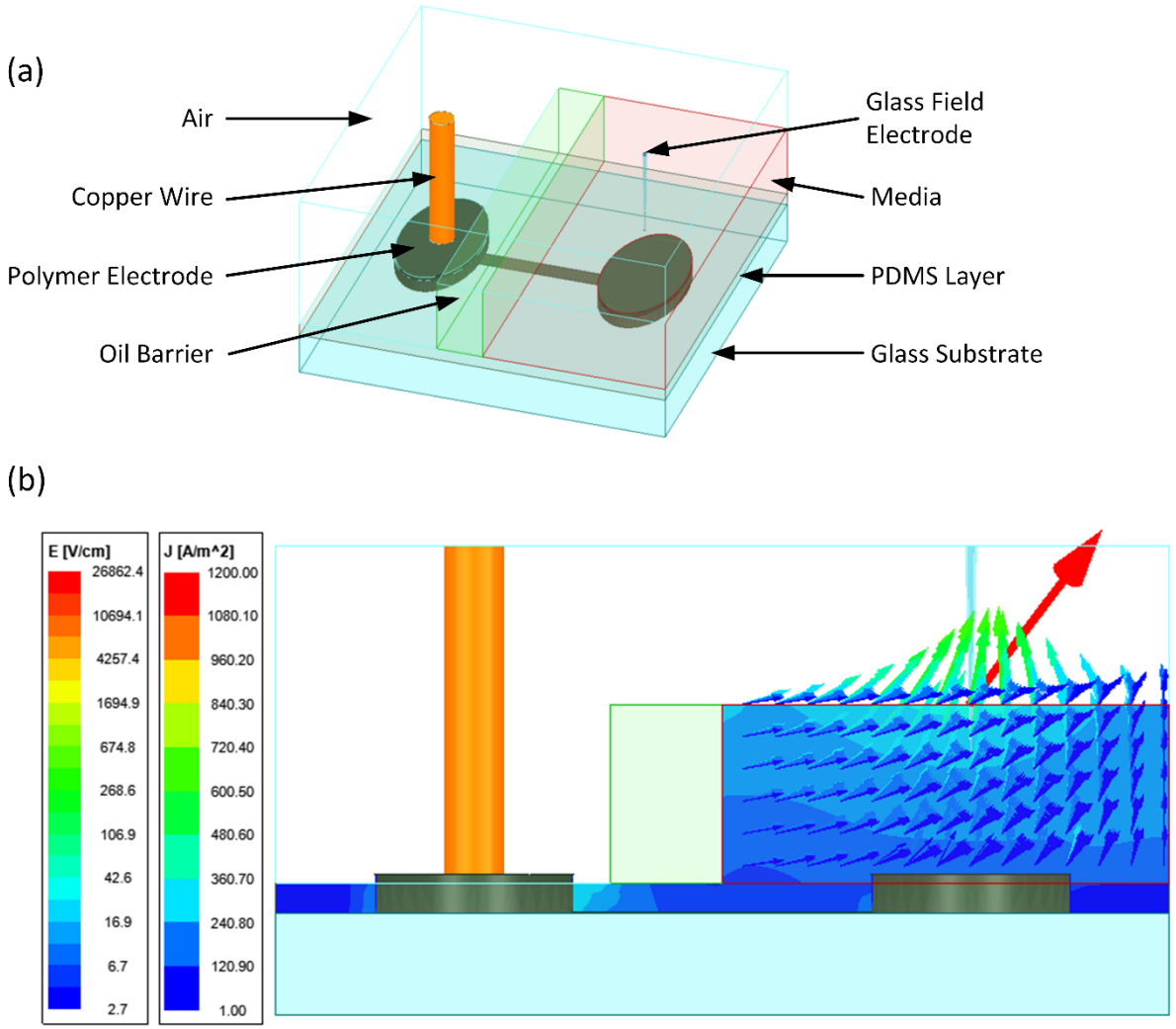

Figure 4. (a) Schematic of EM field simulation. (b) Magnitude of electric field (contour plot) and current density (vector plot) as stimulation is initially applied.

To demonstrate that the conducting polymer electronics integrated in PDMS can be used as neural interfaces, we used the electrodes to stimulate a slice of mouse brain *in vitro*. The electrodes were positioned to stimulate the Schaffer collaterals in the *stratum radiatum* and a single CA1 pyramidal neuron was patch clamped using standard methodology, permitting CA3–CA1 synapses to be recorded (**Figure 5**). A square potential step of 10 V was applied for 80 µs to the PDMS electrode. While the stimulus artifact was wider than that typically obtained with a conventional glass stimulating electrode, a corresponding physiological response was evoked by the PDMS electrode (**Figure 5**, left trace), indicating that the electrodes interact with the nervous system. Importantly, typical CA3-CA1 synaptic properties were observed, whereby application of two stimuli at a 50 ms inter-pulse interval resulted in paired-pulse facilitation i.e., the second response was larger than the first,

reflective of the low initial probability of presynaptic release of the neurotransmitter glutamate at these synapses. Moreover, as would be expected for excitatory currents in the central nervous system, a competitive antagonist of the postsynaptic α-amino-3-hydroxy-5-methyl-4-isoxazolepropionic acid (AMPA)/kainate class of glutamate receptors, 6-cyano-7-nitroquinoxaline-2,3-dione (CNQX), completely abolished the synaptic response, leaving only the stimulus artifact (**Figure 5**, right trace), indicating that the evoked responses are physiological and indeed synaptic in nature.

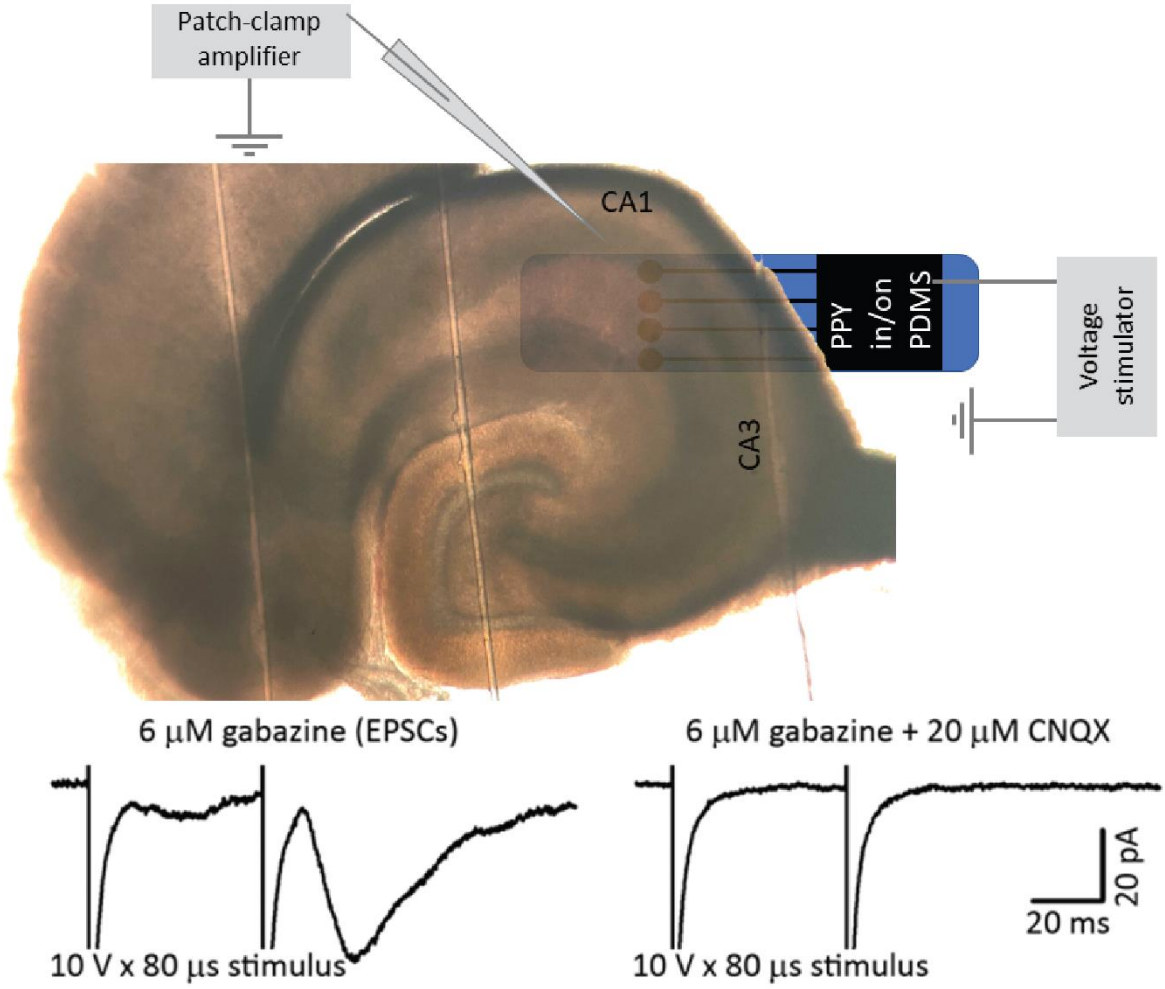

Figure 5. Top) Placement of an *in vitro* hippocampal brain slice on top of a schematic of a PDMS array, such that electrodes contacted presynaptic CA3 axons (Schaffer collaterals). Postsynaptic responses to action potentials evoked in the Schaffer collaterals by a square voltage pulse applied via the PDMS electrodes were recoded from a CA1 pyramidal neuron using a patch electrode in whole-cell voltage-clamp configuration. **Bottom, left)** The $GABA_A$ receptor antagonist gabazine was applied to block inhibitory currents, revealing a purely glutamatergic excitatory postsynaptic current (EPSC). Paired stimuli resulted in paired-pulse

facilitation; the typical form of short-term plasticity displayed at these synapses. **Bottom, right)** The glutamatergic nature of the synaptic response was confirmed by application of an antagonist of AMPA/kainate subtypes of glutamate receptors, CNQX, which abolished the synaptic response, leaving only the stimulus artifact.

Printed electronics integrated in flexible substrates such as those described herein have significant potential for technical applications (e.g., display technologies) and medical applications (e.g., patient specific implantable electrodes for interaction with the central/peripheral nervous system). Printing conducting polymer structures integrated in shape-memory polymer-based materials may facilitate the development of switches, nerve cuff electrodes, etc.,[42,89-94] and proof-of-concept it would be possible to realize such applications was demonstrated by printing PPY structures in/on thin films of an optically transparent SMP (shape-memory polyimide, **Figure S6**).[95]

2.2. Additive manufacturing of conducting polymer-based electronics integrated in 3D objects *in vivo*.

Researchers have previously generated abiotic conducting polymers using electropolymerization in the vicinity of live cells,[96] or indeed oxidative enzymes present in plants [97-99] and invertebrate *Hydra*,[100] in analogy to the production of natural melanins in a variety of organisms.[101] Multiphoton fabrication has been used to print free-standing conducting polymer structures used as an interface for mouse brain slices *in vitro*,[41] and to print non-conducting polymer-based hydrogels in the vicinity of live cells *in vitro*,[102] and *C. elegans*,[103] observing relatively low levels of cytotoxicity over the short timeframe of the experiments. The direct printing of conducting polymer structures directly on/in living organisms would enable real-time repairs of implanted bioelectronic devices and other applications (e.g., miniaturization/customization, precisely controlled reconfiguration of the electronics),[104] however, it has not yet been reported in the literature.[105] To facilitate proof-of-concept that such a technological leap is within reach and it would be possible to realize such applications, we applied multiphoton fabrication to print PPY-based structures on/in live *C. elegans* (**Figure 6**), which complements reports on printing of non-conductive polymer structures employing near infrared (NIR) light sources.[106,107] We chose *C. elegans* for ethical reasons, but also for its high sensitivity to heat, desiccation, and physical injury, making it an ideal testing ground for biosafe laser-based *in vivo* printing approaches in biomedicine. Achieving laser-printing on/in live *C. elegans* would require the lowest possible laser power

that enables ink polymerization, and biocompatible ink components. The PPY-based formulations described earlier were thus first evaluated for *C. elegans* toxicity in order to design a biocompatible ink. While the photo-polymerized ink is inert and non-toxic, future biomedical applications would involve tissue exposure to the unpolymerized mixture prior to *in vivo* printing. It was thus necessary to determine the toxicity of each individual ink component in solution. Two toxicity assays were performed to measure (1) acute adult toxicity and (2) chronic developmental toxicity, for various concentrations of each compound. The former involves exposing adult worms to compounds for 24-48h and relies on the label-free automated survival scoring (LFASS) technique,[108] which exploits the fact that worms fluoresce in blue when they die to pinpoint median time of death.[109] The latter assesses the timing and duration of *C. elegans* successive larval stages and ability to reach reproductive age, using a transgenic strain that produces bioluminescence when the worm is metabolically active.[110] As worms progress through the four larval stages, they feed at increasing rates (commensurate with their size) and produce more bioluminescence. Between larval stages, worms undergo moults during which they cease feeding and appear metabolically quiescent, giving out little bioluminescence. Time-lapse recording of bioluminescence thus enables timing and measurement of developmental stages as bioluminescence rises and falls.

Acute adult toxicity assays revealed that all ink components are acutely toxic at concentrations of 6, 8 and 10 mg/mL but not below 3 mg/mL (**Figure S7**), while only CSA remained acutely toxic at 4 mg/mL. Conversely, neither of the compounds showed any strong developmental toxicity across the range of concentrations tested (10 μg/mL down to 156 ng/mL), as they all allowed worms to reach adulthood in a timely manner (**Figure S8**); although higher doses (2.5-10 μg/mL) of Irgacure, Pyrrole and PEG led to modest developmental shifts (**Figure S9**). These results indicated that the PPY ink components in solution were compatible with *in vivo* printing when employed at concentrations below 4 mg/mL. In particular, HA revealed more biocompatible than CSA and was thus chosen as photoinitiator in the subsequent phases of ink formulation refinement.

Next, to dilute ink component down to biocompatible concentrations, and because *C. elegans* would not naturally consume the ink alone, ink formulations were mixed with dietary E. coli OP50 bacterial paste. As ink dilution into bacterial paste is expected to impact printing performance, several ink to bacterial paste ratios were tested to determine the lowest ratio compatible with live laser-printing. Ink to bacterial paste ratios at 1:1 to 1:10 were tested first on polydimethylsiloxane (PDMS)-coated coverslips and the fidelity of intended printed structures was assessed (**Figure S10**). While sub-millimetric structures could be printed at

1:10 ink to bacterial paste ratios (**Figure S10A-C**), resolving 10-30-micron scale structures was only fully achieved with pure ink formulations (**Figure S10D-F**).

C. elegans were then exposed to HA-based ink formulations mixed with dietary *E. coli* OP50 bacterial paste at 1:5 ratios as a compromise between biocompatibility and printing resolution. Lower-energy infrared two-photon 3D printing was chosen to reduce phototoxicity while enabling deeper tissue penetration (**Figure S11**). Two formulations were tested with subtoxic (3.3 mg/mL, **Figure S11C**) or mildly toxic (6.6 mg/mL **Figure S11A-B, S11D**) Irgacure concentrations. 6-10 μm size square and star shapes were then printed directly onto the skin and within the gut of live *C. elegans* roundworms (**Figure 6**). Thanks to the autofluorescence properties of the ink mix, the printed shapes were imaged and localized by confocal fluorescence imaging, demonstrating accurate and well-tolerated printing of polymer on live worms (**Figure 6 and S11**). Printing within the moving gut of the worm did not yield the intended shape (**Figure 6C**). Faster printing could resolve this limitation, which may be achieved by improving the ink formulation photo-curing efficacy, and/or increasing laser power. However, as light propagates within a complex environment (here the body of the worm), printing accuracy and precision also decreases. Corrective strategies employing adaptive optics will thus likely be necessary to circumvent the issue when translating the approach to thicker vertebrate/human tissues; nevertheless, this represents a technological leap from examples of printing non-conductive structures *in vivo*.[106,107]

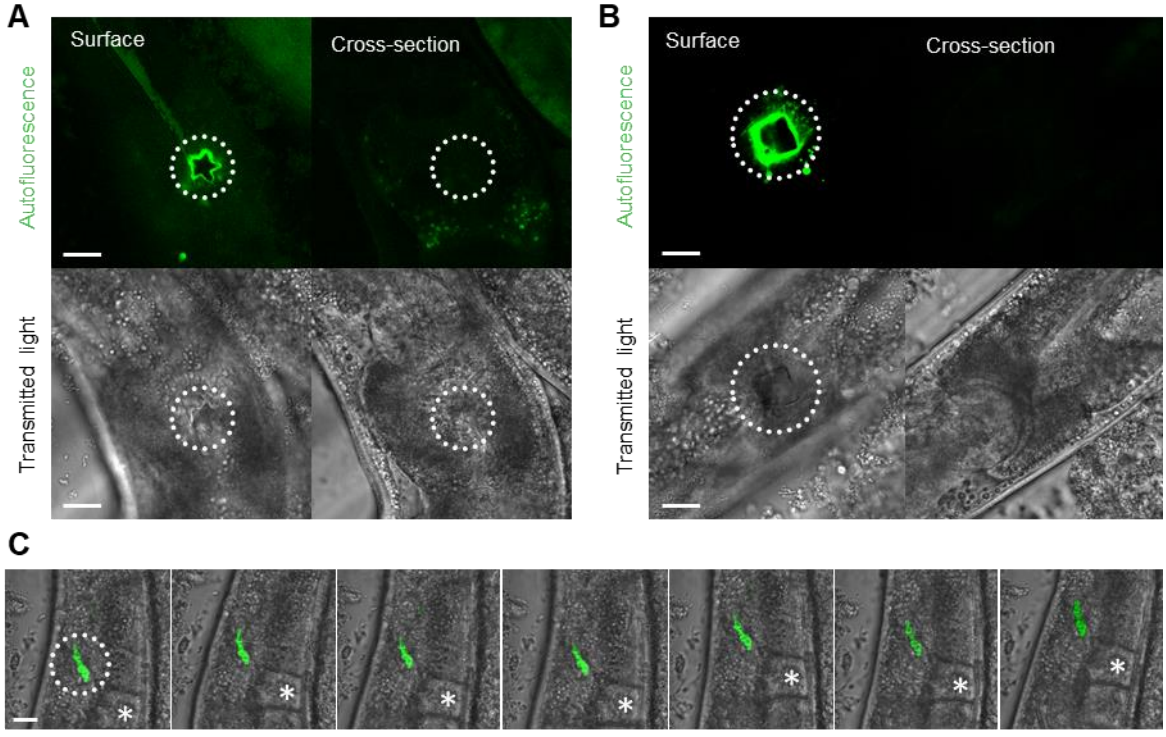

Figure 6. 3D printing of photoresist in live *C. elegans*. (A) 6 µm-wide and 10 µm thick star shape printed onto the cuticle of an anesthetized worm's head with a Nanoscribe® Photonic GT700, imaged by confocal fluorescence (Zeiss LSM880, Exc. 488nm, Em. 543nm, top left) and transmitted light imaging at 40X, without damaging the worm (internal structures intact, right bottom panel). (B) 10 µm-wide and 10 µm thick square shape printed onto the cuticle of a worm. (A-B) Confocal fluorescence (~0.8 µm depth Z-resolution) images of the surface vs cross-section structures are taken 6 µm apart. (C) Time series of images taken 1.5 s apart in a fixed field of view, following attempted printing of a star shape inside the posterior gut lumen of a live worm that had absorbed a 1:5 mix of ink/photoresist and bacterial paste. Live worm movements limited printing accuracy leading to the printing of a somewhat irregular shape. Dotted circles indicate locations of printed structures. Asterisks mark the position of the terminal oocyte. Animals were alive following 3D printing. Scale bars represent 10 µm.

2.3. Ethics.

The research described in this paper has carefully negotiated the ethically sensitive aspects of the experimentation it entailed. For example, *C. elegans* was chosen as a model organism for the *in vivo* experimentation because it does not need ethical approval to use. In addition, the toxicity of the compounds used in the 3D printing process occur on such a small scale that there is a negligible risk of harm to the researchers or the environment. One potential concern is that as future stages of this research progress, there may be a growing scientific case to experiment on more complex organisms (e.g., mice) *in vivo*, and eventually in humans. Given the novel nature of this technology, some may find the thought of first-in-mammal or first-in-human research to be ethically unsettling. However, if this research did reach more advanced stages that required more complex organisms for experimentation, this process would necessarily follow all the typical required safety, ethical and legal protocols. This would be no different than the development of a novel medical device or an analogous scientific procedure.

While the research carried out in this study is not particularly ethically contentious, there is nevertheless a need to be aware of the potential for 'dual-use dilemmas' to emerge as research progresses and becomes more ethically complex. A dual-use dilemma is an ethical dilemma that occurs when research is undertaken with a beneficial use in mind, however, the researchers also foresee that other users may employ this research in ways that could do harm.[111] When it comes to the scientific research outlined in this paper, the authors do not yet feel that the research has reached a point where it could be deployed in ways that could cause

harm. However, if this research maintains a successful trajectory, the potential applications it may have at later stages will grow, and some of these applications may carry the risk of harm if misused. For example, human-computer interfaces could be used to beneficially treat medical patients with neurological conditions; however, such technology could also be used by a bad actor in such a way (e.g., hacking into them to control or obtain information from the device) that negatively affects the privacy and autonomy of the individuals using them.[112-114] One way to responsibly negotiate future dual-use dilemmas is to take steps to try and identify them in advance and subsequently have researchers work with regulators to creatively design ethical safeguards that can be engineered into and alongside the development of the technologies. For example, one safeguarding procedure may involve keeping key aspects of research knowledge secure (e.g., by withholding it) that would otherwise enable the harmful use of such research. Insofar as possible, researchers will need to endeavour to continue to engage in horizon scanning in relation to future stages of this research in order to identify and address ethical dilemmas in advance.

3.0. Conclusion.

Here we report the application of a multiphoton fabrication process to create 3D objects with integrated electronics: *in silico* toxicity screening of ink components identifies/confirms likely cytocompatible formulations; 3D printing through light-transmitting materials yields well-resolved conductive micron-scale features; stimulation of 3D printed PPY structures interfaced with live brain tissue can induce specific synaptic responses; and it is possible to 3D print PPY structures directly *in vivo*.

We showcase a range of examples made by this technology-driven manufacturing (Industry 4.0) process, including PDMS films and a living organism (*C. elegans*); and highlight potential applications such as electrodes capable of stimulating nerve tissue. We foresee significant potential for this technique's integration in human-centric design and bespoke manufacturing (Industry 5.0) processes of producing bioelectronics for telemedicine, and that this represents a possible roadmap for the broader development of direct-printing of electronic devices for biomedical applications in situ.

Computational approaches (e.g., including *in silico* toxicity screening, multiscale modelling of electrical/mechanical/physicochemical properties, etc.) will facilitate ink formulation development for the production of 3D objects with integrated electronics, offering insights into the properties (e.g., electrical conductivity) of the conjugated polymers which underpins their function in devices. Simulation of the interactions between oligomers of components in

the bioelectronic devices (in this case, PDMS, PEG and PPY in water, mimicking the hydrated state of the bioelectrodes if used *in vitro* or *in vivo*) would offer insight into aggregation/clustering due to intramolecular/intermolecular interactions, and potentially phase separation of polymer phases (e.g., associative phase separation). In the long term we believe that such an approach may offer insights that accelerate the discovery, manufacture and deployment of complex composites used in advanced materials technologies generated by additive manufacturing approaches, for example, component selection and composition tuning to achieve optimal properties and device performances.

The potential technical advantages of electronics produced via this technique include (but are not limited to): more accurate targeting (fewer cells stimulated/recorded from) to minimise adverse effects (e.g., tissue damage, immunological reaction/inflammation); increased specificity, efficiency, and effectiveness, with potential of more simultaneous sites for stimulation or recording with optimised signal to noise ratios. Such properties are clinically relevant in the design of implantable bioelectronic devices. With increasing populations and ageing populations worldwide, there are concomitant increases in the number of patients suffering from neurodegenerative conditions (including Parkinson's disease) and other conditions that increase with ageing (e.g., epilepsy, strokes), as well as rises in traumatic brain injury. In this context, potential applications of the approach described herein may include: improved electrodes (smaller, lower morbidity, better tolerated etc.) for deep brain stimulation (e.g., treating Parkinson's disease, epilepsy, etc.), improved monitoring/diagnosis (e.g., advanced epilepsy work-up to identify epileptogenic focus), novel neuroprosthetics (e.g., for traumatic brain injury), new approaches to monitoring/treatment of (peripheral) neuromuscular disorders (e.g., degenerative muscular and peripheral nerve conditions), novel approaches to neuromodulation for pain. In short, we foresee the technique described herein as having significant potential for technical and medical applications, with potential economic, environmental, health and societal impacts.

4.0. Experimental Section.

Materials: Aluminum oxide (basic, Brockmann I, for chromatography, 50-200µm 60A) from Acros organics. (±)-Camphor-10-sulfonic acid, and polyethyleneglycol (Mn 10 kDa) was purchased from Alfa Aesar. Carl Zeiss® Immersol® Immersion Oil, coverslips and polydimethylsiloxane (PDMS, Dow Sylgard 184 Kit) was purchased from Thermo Scientific. Glue (HERMA GmbH) was purchased from Amazon. Unless otherwise stated, everything was purchased from Sigma Aldrich and used as supplied (e.g., polyethylene glycol

dimethacrylate Mn 2 kDa, pyrrole, 2-hydroxy-4-(2-hydroxyethoxy)-2-methylpropiophenone (Irgacure D-2959)).

PDMS substrate preparation: Glass substrates (typically cover slips of ca. 170 µm thickness) were cleaned by submersion in acetone (1 minute), then isopropanol (1 minute), and dried under N_2. Dow Sylgard 184 silicone elastomer curing agent (1.2 g) was added to Dow Sylgard 184 silicone elastomer base (12 g) in a disposable centrifuge tube in the ratio and the mixture was stirred with a spatula and then inverted (10 seconds, 30 times) to ensure thorough mixing of the two components. The PDMS precursor mixture was placed under vacuum in a vacuum desiccator for 30 minutes to remove any air bubbles, after which 1 mL of the PDMS precursor mixture was placed on a glass coverslip attached to a spin coater (Laurell WS-650-23NPPB spin coater) by vacuum, the spin coater lid was closed, parameters selected from **Table S2**, and the spin coater started, and after completion of the steps the coverslips were placed in an oven (90 °C, ca. 3 hours) yielding films with a range of thicknesses of PDMS (summarized in **Table S2**).

In silico toxicity screening: *In silico* toxicity screening was carried out using Derek Nexus (v. 6.0.1, Nexus: 2.2.2) and Sarah Nexus (Sarah Nexus: 3.0.0, Sarah Model: 2.0) supplied by Lhasa Limited, Leeds, UK.

Ink formulation for 3D printing in/on PDMS: A saturated PY-based ink formulation was prepared composed of: pyrrole (1 mL, purified by passage over basic alumina), irgacure D-2959 (250 mg), polyethyleneglycol (10 kDa, 1 mg), polyethyleneglycoldimethyacrylate (2 kDa, 1 mg), camphorsulfonic acid (330 mg). The ink was sonicated for ca. 25 min in the dark at room temperature to ensure mixing, left to rest for ca. 25 min in the dark for any insoluble material to settle, after which the clear upper layer (saturated with monomer, initiator and dopant) was used for printing.

3D printing in/on PDMS: The PDMS-coated coverslips were mounted onto a Nanoscribe® 30 mm coverslip holder made of aluminum with the PDMS-coated side facing downwards. Herma glue was dotted around the edges of the coverslip binding it to the holder and left to dry (10 minutes). A drop of immersion oil was placed on to the glass side of the coverslip. The holder was then flipped so that the PDMS/resist face is upwards and oil face is downwards. A drop of one of the clear ink stock solutions was placed on the substrate and left for 5 minutes to infiltrate the PDMS. The structures to be printed were designed using the computer aided design (CAD) package (Fusion360 from AutoCAD:Autodesk), the structures were exported to the Nanoscribe® software (DeScribe) to do the scripting. The Nanoscribe® Photonic Professional GT 700 instrument was equipped with a light source (Topica

FemtoFiber pro, Er-doped fiber laser of wavelength 780 nm, pulse duration <150 fs, repetition rate 100 MHz, an aperture of 7.3 mm, a diode voltage of 1.34-5, and 50 mW power at the focus point at 100% power). The Nanoscribe® was controlled by the Nanowrite software (version 1.8.14) and the camera software within the Nanoscribe® is AxioVision LE (version 4.8.2.0). The structures were printed on PDMS-coated glass slides using Galvo writing mode by moving beam fixed stage (MBFS) - a fast layer-by-layer writing approach, suitable for micrometre to millimetre scale structures with a computer-controlled piezoelectric scanning stage range 300 x 300 x 300 μm^3. Positioning was achieved using a computer-controlled motor stage, range 100 x 100 mm^2. Laser power and speed for printing on PDMS-coated glass substrates the laser power was ca. 50-60 % and the speed was ca. 5000 µm/s. After printing structures, the substrates were washed with water-ethanol and water to remove low molecular weight contaminants, and the structures were dried under N_2.

Electrical measurements: Direct electrical characterization of the structures was performed using a Keithley 2602B source measure unit, connected to a Wentworth Laboratories SPM197 probe station, with tungsten probes with a 1µm tip diameter. Each wire was swept in a range from 0V to +1V DC. 900 x 40 x 8 µm CSA-doped conductive wires were fabricated within PDMS using 2PP, with circular pads (75 µm diameter) to aid electrical measurements. The electrical properties of the wires were measured with a source-measure unit connected to a probe station. The wires exhibited linear conductance. Their resistance was calculated to be $R_{PPy} = 570 \pm 50$ kΩ. Modelling of the structure, we can estimate the resistivity of the wires using:

$$\sigma = \frac{1}{\rho} = \frac{1}{R}\frac{A}{l}$$

Where R is the measured resistance of the structure, l is the length of the resistor, and A is it's cross-sectional area. The doped PPy structures had $\sigma_{PPy} = 3.9 \pm 0.3$ S/m.

Scanning electron microscopy (SEM) and energy dispersive X-ray spectroscopy (EDX): Samples were mounted on stubs and coated with a layer of gold (ca. 5 nm, 60 s, 20 mA, 8 × 10^{-2} mBar) using a Quorum Q150RES sputter coater (Quorum Technologies Ltd., Lewes, UK). Images were obtained using a JEOL JSM-7800F (Field Emission SEM, FE-SEM) fitted with an EDX system (X-Max50, Oxford Instruments, Abingdon, UK) at 10 mm working distance and 10 kV voltage, three measurements were performed per sample and average results are presented.

Fourier transform infrared (FTIR) spectroscopy: Infrared spectroscopy was carried out on Agilent Cary 630 FTIR Spectrometer. Spectra were recorded in ATR mode, with a 1 cm^{-1}

resolution and 64 scans (corrected for background and atmosphere using OMNIC software supplied with the spectrometer).

Optical coherence tomography (OCT): A line-field optical coherence tomography (LF-OCT) system was employed to measure the electrode sample. The LF-OCT can acquire cross-sectional images (B-scan) in a single shot,[115] which can significantly reduce the motion-induced image distortion and artefacts. The resolution of our system is 8μm axially and 17.5 μm laterally, which enables high-resolution tomography and topography imaging. **Figure S1** shows the LF-OCT system setup, which uses a superluminescent diode (SLED) source to generate low-coherence light centered at 840 nm with 50 nm spectral bandwidth. A beamsplitter (BS) is used to split the optical light into sample arm and reference arm. Line illumination on the sample is achieved by using a cylindrical lens (CYL) and objective lens (L2) resulting in a focused thin line of approximately 7 mm. As the setup uses a Linnik interferometer configuration, the sample arm uses the same optics as the reference arm. The backscattered light from the two arms are recombined at the BS for collection by an imaging spectrograph. By scanning the sample across the y axis, a stack of raw two-dimensional (2D) interferograms at various lateral positions can be acquired yielding a raw 3D data cube. Even though a LF-OCT system has been demonstrated, without a loss of generality, other OCT variants could also be used such as a spectral-domain OCT[116,117] and full-field OCT,[118] though at longer data acquisition time.

Simulations of field stimulation experiments: CSA-doped PPY electrode structure is defined as in **Figure 3** (left) integrated with a PDMS layer (50 μm thick) on a borosilicate glass (relative permittivity 5.5, perfectly insulating) cover slip of ca. 170 μm thickness. Polymer electrode material taken as PPY with conductivity 3.86 S/m. Conductivity of PDMS taken as 2.4×10^{-14} S/m and relative permittivity as 2.5.[119] Glass field electrode formed from pulled borosilicate glass capillary filled with artificial cerebrospinal fluid assumed to have the same conductivity as the media used in the tissue (0.33 S/m). Tip of glass electrode positioned 200 μm vertically above center of end oval of polymer electrode. Glass electrode tip opening has a diameter of 1 μm. Tissue and media held in place by ring of oil (perfectly insulating) of ca. 170 μm thickness and 300 μm high (same height as tissue layer). Voltage applied to exposed end of electrode by copper wire 100 μm diameter (conductivity of 58 MS/m). Stimulation was a constant voltage (20 V, 20 μs) applied to the copper wire with the exposed end of the media in the glass field electrode being set as ground (experimentally this terminal would be a Ag/AgCl wire connecting back to the amplifier). Mesh consisted of 182872 tetrahedral

elements with a maximum element length of 50 μm on polymer electrode and tissue. Simulated for 20 μs (initial step 0.005 μs, max. step 1 μs).

Brain slice preparation and electrical stimulation: Transverse hippocampal brain slices were prepared from a 22-day old C56BL/6J mouse, in accordance with the Animal (Scientific Procedures) Act 1986. Slices of 300 μm were cut and bathed in artificial cerebrospinal fluid (ACSF), containing: NaCl 125 mM, KCl 2.4 mM, $NaHCO_3$ 26 mM, NaH_2PO_4 1.4 mM, D-glucose 20 mM, $MgCl_2$ 1 mM, $CaCl_2$ 2 mM, ca. 315 mOsm/L, pH 7.4, bubbled with 95% O_2/5% CO_2 continuously superfused at a rate of ~2 mL/min The stimulating electrode was a PPY contact pad with a PPY wire spanning the gap to another PPY contact to which a copper wire was attached with conductive silver epoxy cement. The metal surfaces were coated with waterproof nail varnish (an electrical insulator), and a circle of vacuum grease (also an electrical insulator) was drawn around the electrode to make a well in which ACSF could be held. The stimulating electrode was positioned to stimulate Schaffer collaterals in the *stratum radiatum* of CA1 and secured in place on top of the array by nylon strings attached to a loop of platinum wire. The recording electrode (final resistance ca. 5 MΩ) was pulled from a borosilicate glass capillary (1.5 mm outer diameter, 0.84 mm inner diameter; World Precision Instruments) and filled with a patch clamp electrolyte consisting of CsCl 140 mM, HEPES 5 mM, EGTA 10 mM, Mg-ATP 2 mM, pH 7.4, ~295 mOsm/L and whole cell voltage clamp recordings were then made according to standard methods.[120] The patch clamp set up consisted of an EPC9/2 patch clamp amplifier (HEKA Elektronik Dr Schulze GmbH, Lambrecht/Pfalz Germany) connected via the built-in ITC-16 digitizer board to a computer running Pulse software (version 8.80, HEKA); currents were amplified 10×, sequentially low-pass filtered at 10 kHz then 3 kHz and digitized at 10 kHz. Stimulation was controlled within the Pulse software and delivered via a Grass SD9 constant voltage stimulator (10 V x 80 μs). All recordings were made in the presence of 6 μM gabazine (HelloBio, UK), an antagonist of type A γ-aminobutyric acid (GABA) receptors, to isolate excitatory postsynaptic currents. The α-amino-3-hydroxy-5-methyl-4-isoxazolepropionic (AMPA) and kainate subtypes of glutamate receptors were blocked by bath application of 6-cyano-7-nitroquinoxaline-2,3-dione (CNQX; Tocris, UK).

3D printing in SMPs: Optically transparent shape-memory polyimide (TSMPI) was prepared by adaptation of the literature[95] to include a doctor blade step to deposit films of ca. 40 μm in thickness on glass slides. Structures were printed using an ink formulation (composed of pyrrole (50 μL, purified by passage over basic alumina), ethanol (950 μL), Irgacure D-2959

(10 mol % concentration relative to pyrrole)) with laser writing powers of ca. 80-100 %, followed by ethanol washing, yielding structures depicted in **Figure S6**.

Ink formulation for 3D printing in vivo: pyrrole (1 mL, purified by passage over basic alumina), irgacure D-2959 (50 mg), polyethylene glycol (10 kDa, 1 mg), polyethylene glycol dimethyl-acrylate (2 kDa, 1 mg), hyaluronic acid (50mg). The inks were sonicated for ca. 25 min in the dark at room temperature to ensure mixing, left to rest for ca. 25 min in the dark for any insoluble material to settle, after which the clear upper layer (saturated with monomer, initiator and dopant) was either used for toxicity screening (death fluorescence,[109] or bioluminescence developmental assays)[110] or mixed with *E. coli* OP50 bacterial paste and used for printing either in PDMS (as described above) or *C. elegans* (as described below).

C. elegans acute adult toxicity testing: Worms were synchronized by bleaching and raised at 20 ℃ on *E. coli* OP50-seeded nematode-growth medium plates as previously described[121] until they reached L4 stage. L4 worms were then transferred to new *E. coli* OP50-seeded nematode-growth medium plates at 25 ℃ for 24h before processing them for survival assays. Photoresist component stock solutions in DMSO were diluted serially in M9 buffer to yield the concentrations tested. Assays were run and analyzed as previously described[108], substituting the oxidant *t*-BHP with the photoresist component solutions.

C. elegans developmental toxicity testing: Worms were synchronized by bleaching and raised at 20 ℃ on *E. coli* OP50-seeded nematode-growth medium plates as previously described.[121] To assess chronic developmental toxicity, synchronized L1 worms were collected in sterile M9 buffer, washed three times in M9, and the worm concentration of the resulting solution was determined by counting the number of worms in four 10 μL drop of solution under a stereomicroscope at 40X magnification. Photoresist component stock solutions in DMSO were diluted serially in M9 buffer to yield the concentrations tested. The developmental assay was adapted from Olmedo et al.[110] Briefly, ~20 worms per well and a 2-3 μL bacterial pellet were dispensed in 30 μL of M9 in each well of a 384 well white microplate. Following dispensing of worms and bacteria in all wells, 8 μL of each test solution and 40 μL of 2x luciferin solution (for final concentration see literature)[110] were added to each well. Bioluminescence measurements were carried out every 6 min as described[110] for up to 72h in a Tecan Infinite M200 Pro (Tecan Ltd.). Readouts were plotted and analyzed blind in Microsoft Excel 365 to determine the timings and lengths of larval stages. Statistics performed used two-way ANOVA with post-hoc Dunnett's correction for multiple comparisons.

PDMS groove preparation for 3D-printing on C. elegans: To trap worms while printing onto or inside them, a thermally resilient and optically clear matrix is needed. The 2-4% agarose pads used in traditional setups for *C. elegans* microscopy observations was thus substituted for 75 μm thin PDMS films. PDMS (Sylgard 184, Farnell) at 14:1 base to curing agent ratio was spin-coated at 700 rpm on 12-inch vinyl record chunks (typically 2-3 inches wide) for 1 min, baked at 60°C for 3h, cut in 1 cm^2 slabs, and bound to 22 mm and 30 mm diameter coverslips using oxygen plasma activation of silicon surfaces. Coated coverslips were stored in a dust-free environment until use. Before use, they were briefly rinsed with isopropanol and dried with an air gun.

3D printing in vivo in C. elegans: Wildtype *C. elegans* Bristol N2 worms were maintained as previously described.[121] Synchronized day 1-old adult worms were then fed a 1:5 mixture of ink/photoresist and concentrated *E. coli* OP50 bacterial paste (100 times concentrated from a OD_{600} nm = 1 solution in lysogenic broth) dispensed and spread (after homogenization by vortexing 20 s following a 30 min incubation at 30°C) at 200 μL per 6 cm Nematode Growth Medium Agar plate, for 1 hour at 25°C. Worms were then immobilized in 0.2% levamisole prepared in a 2 μL drop of an even mix of 1:10 mixture of photoresist and concentrated OP50 and M9 medium, between two 1 cm^2 slabs of PDMS grooves bonded onto a 22 mm-diameter and a 30 mm-diameter coverslips (PDMS film were prepared by spin-coating at 700 rpm on vinyl records for 1 min, baked at 60°C for 3h, cut in 1 cm^2 slabs, and bound to coverslips by plasma-cleaning). During worm mounting, worms were aligned inside the grooves using a platinum pick, and vacuum grease was used to seal the edges of the coverslips. Coverslips were then mounted into the Nanoscribe® holder (Herma glue was dotted around the edges of the coverslip binding it to the holder and left to dry for 10 minutes) and a drop of immersion oil (immersol 518F) was applied. The sample was then processed for 3D nano-printing through a Zeiss 63X 1.4NA lens from a Nanoscribe® Photonic Professional GT 700 instrument operating in galvo mode at speeds of 500-1,000 μm/s with a laser power output of 40 – 60 mW (Topica FemtoFiber pro Er-doped fiber laser with a pulse duration <150 fs, a repetition rate of 100MHz, a wavelength of 780 nm, an aperture of 7.3 mm and a diode voltage of 1.34-5).

Confocal imaging of C. elegans: Following 3D printing, worms were collected by transferring the coverslips onto a microscopy slide with M9 added to prevent desiccation. The slides were then imaged through a Zeiss 40X 1.4NA oil immersion lens with a Zeiss LSM880 confocal microscope exciting the sample at 488nm and collecting fluorescence signal at 543nm and operated by the Zen Black software. Z-stacks were acquired at 1024x1024 $pixel^2$ every 0.45

µm across the first half of the worm thickness (about 30 µm). single plane sequences were acquired at maximum speed (1.5 s per frame after averaging). Images were then exported and processed with FiJi for figure preparation.[122]

Supporting Information

Supporting Information is available from the Wiley Online Library or from the author.

Acknowledgements

J.G.H. thanks the UK Engineering and Physical Sciences Research Council (EPSRC) for financial support (Grant References: EP/R003823/1 and EP/R511560/1, that supported G.R.H.), and the UK Royal Society for financial support (Grant Reference: RG160449). J.G.H. and D.M.C. thank the EPSRC Centre for Innovative Manufacturing in Large-Area Electronics (CIMLAE) for a Pathfinder Grant (Grant Reference: EP/K03099X/1, that supported P.K.), and the UK Biotechnology and Biological Sciences Research Council (BBSRC) Network in Industrial Biotechnology and Bioenergy (NIBB) scheme for a Business Interaction Voucher for supporting interactions with NeuDrive (Grant Reference: BB/L013762/1, that supported G.R.H.). J.G.H. and O.E. acknowledge financial support from European Regional Development Funds (Project Ref: 03R19P03809). H.H.G. acknowledges Erasmus Mundus for financial support. We thank Dstl for financial support (Grant Reference: ACC2019189) that supported M.J.F., S.J.B., D.C., J.B.A., and J.G.H. Z.Z. and Y.S. acknowledge the EPSRC for financial support (Grant Reference: Grant Reference: EP/R014094/1). H.L. acknowledges the EPSRC for financial support (Grant References: EP/R019460/1 and EP/P024807/1). A. B. thanks the Wellcome Trust for financial support (Wellcome Trust Seed Award in Sciences 214076/Z/18/Z, which supported C.A.). J.R.M. was supported by a Lancaster University Faculty of Health and Medicine PhD scholarship. J.G.H. and D.M.C. acknowledge insightful discussions with Professor Frances Edwards at University College London. D.M.C. thanks Alzheimer's Research UK (ARUK) for financial support (Grant Reference: ARUK-PG2019B-018). J.G.H. thanks MRC for supporting interactions with NeuDrive (Grant Reference: MC_PC_17192). J.G.H. acknowledges insightful conversations with Daniel Chew of Galvani Bioelectronics, and Simon Ogier, Kiron Rajeev, Dominique Richardson, Mike Simms, Malcolm Stewart and Jane Theaker at NeuDrive.

Author Contributions

Conceptualization, J.G.H.; methodology, all authors; formal analysis, all authors; investigation, S.J.B., P.K., G.R.H., R.G., H.H.G., M.J.F., Z.Z. & Z.Z., J.R.M., C.A., M.D.A., M.J.H., B.S., D.C., D.M.C., A.B.; data curation, S.J.B., Y.S., B.S., D.C., D.M.C., A.B., J.G.H.; writing—original draft preparation, J.G.H. and A.B.; writing—review and editing, all authors; supervision, Y.S., H.L., D.C., D.M.C., A.B., J.G.H.; project administration, D.M.C., A.B., J.G.H; funding acquisition, Y.S., H.L., D.M.C., A.B., J.G.H.

Received: ((will be filled in by the editorial staff))
Revised: ((will be filled in by the editorial staff))
Published online: ((will be filled in by the editorial staff))

References

1. Tulkoff C, Caswell G. *Design for Excellence in Electronics Manufacturing*. Newark: John Wiley & Sons, Incorporated; 2021.
2. Cagnan H, Denison T, McIntyre C, Brown P. Emerging technologies for improved deep brain stimulation. *Nature Biotechnology*. 2019/09/01 2019;37(9):1024-1033. doi:10.1038/s41587-019-0244-6
3. Cho Y, Park S, Lee J, Yu KJ. Emerging Materials and Technologies with Applications in Flexible Neural Implants: A Comprehensive Review of Current Issues with Neural Devices. *Adv Mater*. 2021;33(47):e2005786-n/a. doi:10.1002/adma.202005786
4. Fanelli A, Ferlauto L, Zollinger EG, et al. Transient neurovascular interface for minimally invasive neural recording and stimulation. *Advanced Materials Technologies*. 2022;7(2):2100176.
5. Frank JA, Antonini M-J, Anikeeva P. Next-generation interfaces for studying neural function. *Nature Biotechnology*. 2019/09/01 2019;37(9):1013-1023. doi:10.1038/s41587-019-0198-8
6. Higgins SG, Lo Fiego A, Patrick I, Creamer A, Stevens MM. Organic bioelectronics: using highly conjugated polymers to interface with biomolecules, cells, and tissues in the human body. *Advanced Materials Technologies*. 2020;5(11):2000384.
7. Kim DC, Shim HJ, Lee W, Koo JH, Kim DH. Stretchable Electronics: Material‐Based Approaches for the Fabrication of Stretchable Electronics (Adv. Mater. 15/2020). *Advanced materials (Weinheim)*. 2020;32(15):2070118-n/a. doi:10.1002/adma.202070118
8. Liu Y, Feig VR, Bao Z. Conjugated polymer for implantable electronics toward clinical application. *Advanced Healthcare Materials*. 2021;10(17):2001916.
9. Luan L, Robinson JT, Aazhang B, et al. Recent Advances in Electrical Neural Interface Engineering: Minimal Invasiveness, Longevity, and Scalability. *Neuron*. 2020/10/28/ 2020;108(2):302-321. doi:https://doi.org/10.1016/j.neuron.2020.10.011
10. Patel SR, Lieber CM. Precision electronic medicine in the brain. *Nature Biotechnology*. 2019/09/01 2019;37(9):1007-1012. doi:10.1038/s41587-019-0234-8
11. Rochford AE, Carnicer‐Lombarte A, Curto VF, Malliaras GG, Barone DG. When Bio Meets Technology: Biohybrid Neural Interfaces. *Adv Mater*. 2020;32(15):e1903182-n/a. doi:10.1002/adma.201903182

12. Shahriari D, Rosenfeld D, Anikeeva P. Emerging Frontier of Peripheral Nerve and Organ Interfaces. *Neuron*. 2020/10/28/ 2020;108(2):270-285. doi:https://doi.org/10.1016/j.neuron.2020.09.025
13. Singer A, Robinson JT. Wireless power delivery techniques for miniature implantable bioelectronics. *Advanced Healthcare Materials*. 2021;10(17):2100664.
14. Yoo J-Y, Yang J-S, Chung M-K, Kim S-H, Yoon J-B. A review of geometric and structural design for reliable flexible electronics. *Journal of Micromechanics and Microengineering*. 2021;31(7):074001.
15. Yoo S, Lee J, Joo H, Sunwoo SH, Kim S, Kim DH. Wireless power transfer and telemetry for implantable bioelectronics. *Advanced healthcare materials*. 2021;10(17):2100614.
16. Zeng Q, Li X, Zhang S, Deng C, Wu T. Think big, see small—A review of nanomaterials for neural interfaces. *Nano select*. 2022;3(5):903-918. doi:10.1002/nano.202100256
17. Zhang M, Tang Z, Liu X, Van der Spiegel J. Electronic neural interfaces. *Nature Electronics*. 2020/04/01 2020;3(4):191-200. doi:10.1038/s41928-020-0390-3
18. Zou M, Ma Y, Yuan X, Hu Y, Liu J, Jin Z. Flexible devices: from materials, architectures to applications. *Journal of Semiconductors*. 2018;39(1):011010.
19. Bettucci O, Matrone GM, Santoro F. Conductive Polymer‐Based Bioelectronic Platforms toward Sustainable and Biointegrated Devices: A Journey from Skin to Brain across Human Body Interfaces. *Advanced Materials Technologies*. 2022;7(2):2100293.
20. Marques-Hueso J, Jones TDA, Watson DE, et al. A Rapid Photopatterning Method for Selective Plating of 2D and 3D Microcircuitry on Polyetherimide. https://doi.org/10.1002/adfm.201704451. *Advanced Functional Materials*. 2018/02/01 2018;28(6):1704451. doi:https://doi.org/10.1002/adfm.201704451
21. Esfahani RN, Shuttleworth MP, Doychinov V, et al. Light based synthesis of metallic nanoparticles on surface-modified 3D printed substrates for high performance electronic systems. *Additive Manufacturing*. 2020/08/01/ 2020;34:101367. doi:https://doi.org/10.1016/j.addma.2020.101367
22. Ryspayeva A, Jones TDA, Esfahani MN, et al. A rapid technique for the direct metallization of PDMS substrates for flexible and stretchable electronics applications. *Microelectronic Engineering*. 2019/03/15/ 2019;209:35-40. doi:https://doi.org/10.1016/j.mee.2019.03.001
23. Manousiouthakis E, Park J, Hardy JG, Lee JY, Schmidt CE. Towards the translation of electroconductive organic materials for regeneration of neural tissues. *Acta Biomaterialia*. 2022/02/01/ 2022;139:22-42. doi:https://doi.org/10.1016/j.actbio.2021.07.065
24. Someya T, Bao Z, Malliaras GG. The rise of plastic bioelectronics. *Nature*. 2016/12/01 2016;540(7633):379-385. doi:10.1038/nature21004
25. Guo X, Baumgarten M, Müllen K. Designing π-conjugated polymers for organic electronics. *Progress in Polymer Science*. 2013/12/01/ 2013;38(12):1832-1908. doi:https://doi.org/10.1016/j.progpolymsci.2013.09.005
26. Nezakati T, Seifalian A, Tan A, Seifalian AM. Conductive Polymers: Opportunities and Challenges in Biomedical Applications. *Chemical Reviews*. 2018/07/25 2018;118(14):6766-6843. doi:10.1021/acs.chemrev.6b00275
27. Chen Y, Zhang Y, Liang Z, Cao Y, Han Z, Feng X. Flexible inorganic bioelectronics. *npj Flexible Electronics*. 2020/02/04 2020;4(1):2. doi:10.1038/s41528-020-0065-1
28. Guo L, Ma M, Zhang N, Langer R, Anderson DG. Stretchable polymeric multielectrode array for conformal neural interfacing. *Advanced materials*. 2014;26(9):1427-1433.

29. Park HL, Lee Y, Kim N, Seo DG, Go GT, Lee TW. Flexible neuromorphic electronics for computing, soft robotics, and neuroprosthetics. *Advanced Materials*. 2020;32(15):1903558.
30. Song E, Li J, Won SM, Bai W, Rogers JA. Materials for flexible bioelectronic systems as chronic neural interfaces. *Nature Materials*. 2020/06/01 2020;19(6):590-603. doi:10.1038/s41563-020-0679-7
31. Cuttaz EA, Chapman CAR, Syed O, Goding JA, Green RA. Stretchable, fully polymeric electrode arrays for peripheral nerve stimulation. *Advanced Science*. 2021;8(8):2004033.
32. Yang Q, Wei T, Yin RT, et al. Photocurable bioresorbable adhesives as functional interfaces between flexible bioelectronic devices and soft biological tissues. *Nature Materials*. 2021/11/01 2021;20(11):1559-1570. doi:10.1038/s41563-021-01051-x
33. Goh GL, Zhang H, Chong TH, Yeong WY. 3D printing of multilayered and multimaterial electronics: a review. *Advanced Electronic Materials*. 2021;7(10):2100445.
34. Layani M, Wang X, Magdassi S. Novel materials for 3D printing by photopolymerization. *Advanced Materials*. 2018;30(41):1706344.
35. Yuk H, Lu B, Lin S, et al. 3D printing of conducting polymers. *Nature Communications*. 2020/03/30 2020;11(1):1604. doi:10.1038/s41467-020-15316-7
36. Alberto P, Bhanu P, Scott AM, et al. Laser direct-write of embedded electronic components and circuits. 2005:223-230.
37. Dadras-Toussi O, Khorrami M, Louis Sam Titus ASC, Majd S, Mohan C, Abidian MR. Multiphoton Lithography of Organic Semiconductor Devices for 3D Printing of Flexible Electronic Circuits, Biosensors, and Bioelectronics. https://doi.org/10.1002/adma.202200512. *Advanced Materials*. 2022/07/01 2022;34(30):2200512. doi:https://doi.org/10.1002/adma.202200512
38. Li L, Fourkas JT. Multiphoton polymerization. *Materials Today*. 2007/06/01/ 2007;10(6):30-37. doi:https://doi.org/10.1016/S1369-7021(07)70130-X
39. Nguyen AK, Narayan RJ. Two-photon polymerization for biological applications. *Materials Today*. 2017/07/01/ 2017;20(6):314-322. doi:https://doi.org/10.1016/j.mattod.2017.06.004
40. Wloka T, Gottschaldt M, Schubert US. From Light to Structure: Photo Initiators for Radical Two‐Photon Polymerization. *Chemistry–A European Journal*. 2022:e202104191.
41. Hardy JG, Hernandez DS, Cummings DM, Edwards FA, Shear JB, Schmidt CE. Multiphoton microfabrication of conducting polymer-based biomaterials. *Journal of Materials Chemistry B*. 2015;3(25):5001-5004.
42. Hardy JG, Palma M, Wind SJ, Biggs MJ. Responsive biomaterials: advances in materials based on shape‐memory polymers. *Advanced Materials*. 2016;28(27):5717-5724.
43. Goding JA, Gilmour AD, Aregueta-Robles UA, Hasan EA, Green RA. Living Bioelectronics: Strategies for Developing an Effective Long-Term Implant with Functional Neural Connections. https://doi.org/10.1002/adfm.201702969. *Advanced Functional Materials*. 2018/03/01 2018;28(12):1702969. doi:https://doi.org/10.1002/adfm.201702969
44. Novikov A, Goding J, Chapman C, Cuttaz E, Green RA. Stretchable bioelectronics: Mitigating the challenges of the percolation threshold in conductive elastomers. *APL Materials*. 2020/10/01 2020;8(10):101105. doi:10.1063/5.0005410
45. Adly N, Weidlich S, Seyock S, et al. Printed microelectrode arrays on soft materials: from PDMS to hydrogels. *npj Flexible Electronics*. 2018/05/24 2018;2(1):15. doi:10.1038/s41528-018-0027-z
46. Bohr A, Memarzadeh K. Chapter 2 - The rise of artificial intelligence in healthcare applications. In: Bohr A, Memarzadeh K, eds. *Artificial Intelligence in Healthcare*. Academic Press; 2020:25-60.

47. Chang AC. Chapter 11 - The Future of Artificial Intelligence in Medicine. In: Chang AC, ed. *Intelligence-Based Medicine*. Academic Press; 2020:431-443.
48. Drew L. The ethics of brain-computer interfaces. *Nature*. 2019;571(7766):S19-S19.
49. Shah P, Kendall F, Khozin S, et al. Artificial intelligence and machine learning in clinical development: a translational perspective. *npj Digital Medicine*. 2019/07/26 2019;2(1):69. doi:10.1038/s41746-019-0148-3
50. Maddikunta PKR, Pham Q-V, B P, et al. Industry 5.0: A survey on enabling technologies and potential applications. *Journal of Industrial Information Integration*. 2022/03/01/ 2022;26:100257. doi:https://doi.org/10.1016/j.jii.2021.100257
51. Manjunatheshwara KJ, Vinodh S. Sustainable electronics product design and manufacturing: State of art review. *International Journal of Sustainable Engineering*. 2021;14(4):541-551.
52. Wang L. A futuristic perspective on human-centric assembly. *Journal of Manufacturing Systems*. 2022/01/01/ 2022;62:199-201. doi:https://doi.org/10.1016/j.jmsy.2021.11.001
53. Butler KT, Davies DW, Cartwright H, Isayev O, Walsh A. Machine learning for molecular and materials science. *Nature*. 2018/07/01 2018;559(7715):547-555. doi:10.1038/s41586-018-0337-2
54. Hardy JG, Sdepanian S, Stowell AF, et al. Potential for Chemistry in Multidisciplinary, Interdisciplinary, and Transdisciplinary Teaching Activities in Higher Education. *Journal of Chemical Education*. 2021/04/13 2021;98(4):1124-1145. doi:10.1021/acs.jchemed.0c01363
55. de Pablo JJ, Jackson NE, Webb MA, et al. New frontiers for the materials genome initiative. *npj Computational Materials*. 2019/04/05 2019;5(1):41. doi:10.1038/s41524-019-0173-4
56. Liu Y, Niu C, Wang Z, et al. Machine learning in materials genome initiative: A review. *Journal of Materials Science & Technology*. 2020/11/15/ 2020;57:113-122. doi:https://doi.org/10.1016/j.jmst.2020.01.067
57. Helmus MN, Gibbons DF, Cebon D. Biocompatibility: Meeting a Key Functional Requirement of Next-Generation Medical Devices. *Toxicologic Pathology*. 2008/01/01 2008;36(1):70-80. doi:10.1177/0192623307310949
58. Lueddeckens S, Saling P, Guenther E. Temporal issues in life cycle assessment—a systematic review. *The International Journal of Life Cycle Assessment*. 2020/08/01 2020;25(8):1385-1401. doi:10.1007/s11367-020-01757-1
59. Ramesh P, Vinodh S. State of art review on Life Cycle Assessment of polymers. *International Journal of Sustainable Engineering*. 2020/11/01 2020;13(6):411-422. doi:10.1080/19397038.2020.1802623
60. Marchant CA. Computational toxicology: a tool for all industries. *Wiley Interdisciplinary Reviews: Computational Molecular Science*. 2012;2(3):424-434.
61. Hemmerich J, Ecker GF. In silico toxicology: From structure–activity relationships towards deep learning and adverse outcome pathways. *Wiley Interdisciplinary Reviews: Computational Molecular Science*. 2020;10(4):e1475.
62. Raies AB, Bajic VB. In silico toxicology: computational methods for the prediction of chemical toxicity. *Wiley Interdisciplinary Reviews: Computational Molecular Science*. 2016;6(2):147-172.
63. Raies AB, Bajic VB. In silico toxicology: comprehensive benchmarking of multi‐label classification methods applied to chemical toxicity data. *Wiley Interdisciplinary Reviews: Computational Molecular Science*. 2018;8(3):e1352.
64. Raunio H. In Silico Toxicology – Non-Testing Methods. Perspective. *Frontiers in Pharmacology*. 2011;2

65. Rim K-T. In silico prediction of toxicity and its applications for chemicals at work. *Toxicology and Environmental Health Sciences*. 2020/09/01 2020;12(3):191-202. doi:10.1007/s13530-020-00056-4
66. Pérez Santín E, Rodríguez Solana R, González García M, et al. Toxicity prediction based on artificial intelligence: A multidisciplinary overview. *Wiley Interdisciplinary Reviews: Computational Molecular Science*. 2021;11(5):e1516.
67. Tropp J, Rivnay J. Design of biodegradable and biocompatible conjugated polymers for bioelectronics. 10.1039/D1TC03600A. *Journal of Materials Chemistry C*. 2021;9(39):13543-13556. doi:10.1039/D1TC03600A
68. Hodgson E, Levi PE. *A textbook of modern toxicology*. vol 274. Elsevier New York; 1987.
69. Ford KA. Refinement, Reduction, and Replacement of Animal Toxicity Tests by Computational Methods. *ILAR Journal*. 2016;57(2):226-233. doi:10.1093/ilar/ilw031
70. Madden JC, Enoch SJ, Paini A, Cronin MTD. A Review of In Silico Tools as Alternatives to Animal Testing: Principles, Resources and Applications. *Alternatives to Laboratory Animals*. 2020/07/01 2020;48(4):146-172. doi:10.1177/0261192920965977
71. Törnqvist E, Annas A, Granath B, Jalkesten E, Cotgreave I, Öberg M. Strategic focus on 3R principles reveals major reductions in the use of animals in pharmaceutical toxicity testing. *PloS one*. 2014;9(7):e101638.
72. Ashton MD, Appen IC, Firlak M, et al. Wirelessly triggered bioactive molecule delivery from degradable electroactive polymer films. *Polymer International*. 2021;70(4):467-474.
73. Distler T, Polley C, Shi F, et al. Electrically Conductive and 3D‐Printable Oxidized Alginate‐Gelatin Polypyrrole: PSS Hydrogels for Tissue Engineering. *Advanced Healthcare Materials*. 2021;10(9):2001876.
74. Magaz A, Ashton MD, Hathout RM, Li X, Hardy JG, Blaker JJ. Electroresponsive Silk-Based Biohybrid Composites for Electrochemically Controlled Growth Factor Delivery. *Pharmaceutics*. 2020;12(8)doi:10.3390/pharmaceutics12080742
75. Edwards AV, Hann C, Ivill H, et al. Additive manufacturing of multielectrode arrays for biotechnological applications. *Materials Advances*. 2021;2(5):1600-1605.
76. Qi D, Zhang K, Tian G, Jiang B, Huang Y. Stretchable electronics based on PDMS substrates. *Advanced Materials*. 2021;33(6):2003155.
77. Ertas YN, Ozpolat D, Karasu SN, Ashammakhi N. Recent Advances in Cochlear Implant Electrode Array Design Parameters. *Micromachines*. 2022;13(7). doi:10.3390/mi13071081
78. Gluth MB, Singh R, Atlas MD. Prevention and management of cochlear implant infections. *Cochlear Implants International*. 2011/11/01 2011;12(4):223-227. doi:10.1179/146701011X12950038111576
79. Copeland M, Choi M, Bleiweiss IJ. Silicone breakdown and capsular synovial metaplasia in textured-wall saline breast prostheses. *Plastic and reconstructive surgery*. 1994;94(5):628-33.
80. Haider SG, Stuhl O, Goslar HG, Birkofer L. Lethal dose estimation and histophysiological effects of an organosilicon compound on rat kidney, liver and testis. *Cellular and molecular biology*. 1983;29(4):299-306.
81. Rücker C, Kümmerer K. Environmental Chemistry of Organosiloxanes. *Chemical Reviews*. 2015/01/14 2015;115(1):466-524. doi:10.1021/cr500319v
82. Kaali P, Momcilovic D, Markström A, Aune R, Czel G, Karlsson S. Degradation of biomedical polydimethylsiloxanes during exposure to in vivo biofilm environment monitored by FE‐SEM, ATR‐FTIR, and MALDI‐TOF MS. *Journal of Applied Polymer Science*. 2010;115(2):802-810.

83. Tohfafarosh M, Sevit A, Patel J, et al. Characterization of outer insulation in long-term-implanted leads. *Journal of long-term effects of medical implants*. 2016;26(3)
84. Jeong J, Chou N, Kim S. Long-term characterization of neural electrodes based on parylene-caulked polydimethylsiloxane substrate. *Biomedical Microdevices*. 2016/05/11 2016;18(3):42. doi:10.1007/s10544-016-0065-z
85. Senzaki T, Fujikawa S. Design of Polymer Coating Materials for Long-term Hydrophilic Stability of Poly (dimethylsiloxane) Surfaces. *Chemistry Letters*. 2019;48(9):1152-1155.
86. Zhang H, Chiao M. Anti-fouling Coatings of Poly(dimethylsiloxane) Devices for Biological and Biomedical Applications. *Journal of Medical and Biological Engineering*. 2015/04/01 2015;35(2):143-155. doi:10.1007/s40846-015-0029-4
87. Au-Yong S, Firlak M, Draper ER, et al. Electrochemically Enhanced Delivery of Pemetrexed from Electroactive Hydrogels. *Polymers*. 2022;14(22). doi:10.3390/polym14224953
88. Elbohouty M, Wilson MT, Voss LJ, Steyn-Ross DA, Hunt LA. In vitro electrical conductivity of seizing and non-seizing mouse brain slices at 10 kHz. *Physics in Medicine & Biology*. 2013;58(11):3599.
89. Fidanovski K, Mawad D. Conjugated polymers in bioelectronics: addressing the interface challenge. *Advanced Healthcare Materials*. 2019;8(10):1900053.
90. Gillis WF, Lissandrello CA, Shen J, et al. Carbon fiber on polyimide ultra-microelectrodes. *Journal of Neural Engineering*. 2018/01/08 2018;15(1):016010. doi:10.1088/1741-2552/aa8c88
91. Haskew M, Hardy J. A mini-review of shape-memory polymer-based materials: stimuli-responsive shape-memory polymers. *Johnson Matthey Technology Review*. 2020;64(4)
92. Lee H, Won Y, Oh JH. Neuromorphic bioelectronics based on semiconducting polymers. *Journal of Polymer Science*. 2022;60(3):348-376.
93. Liang Y, Offenhäusser A, Ingebrandt S, Mayer D. PEDOT: PSS‐Based Bioelectronic Devices for Recording and Modulation of Electrophysiological and Biochemical Cell Signals. *Advanced Healthcare Materials*. 2021;10(11):2100061.
94. Lissandrello CA, Gillis WF, Shen J, et al. A micro-scale printable nanoclip for electrical stimulation and recording in small nerves. *Journal of Neural Engineering*. 2017/03/21 2017;14(3):036006. doi:10.1088/1741-2552/aa5a5b
95. Xiao X, Qiu X, Kong D, Zhang W, Liu Y, Leng J. Optically transparent high temperature shape memory polymers. 10.1039/C5SM02703A. *Soft Matter*. 2016;12(11):2894-2900. doi:10.1039/C5SM02703A
96. Richardson-Burns SM, Hendricks JL, Foster B, Povlich LK, Kim D-H, Martin DC. Polymerization of the conducting polymer poly(3,4-ethylenedioxythiophene) (PEDOT) around living neural cells. *Biomaterials*. 2007/03/01/ 2007;28(8):1539-1552. doi:https://doi.org/10.1016/j.biomaterials.2006.11.026
97. Parker D, Daguerre Y, Dufil G, et al. Biohybrid plants with electronic roots via in vivo polymerization of conjugated oligomers. 10.1039/D1MH01423D. *Materials Horizons*. 2021;8(12):3295-3305. doi:10.1039/D1MH01423D
98. Parker D, Daguerre Y, Dufil G, et al. Correction: Biohybrid plants with electronic roots via in vivo polymerization of conjugated oligomers. 10.1039/D2MH90021A. *Materials Horizons*. 2022;9(4):1317-1318. doi:10.1039/D2MH90021A
99. Stavrinidou E, Gabrielsson R, Nilsson KPR, et al. In vivo polymerization and manufacturing of wires and supercapacitors in plants. *Proceedings of the National Academy of Sciences*. 2017;114(11):2807-2812.

100. Tommasini G, Dufil G, Fardella F, et al. Seamless integration of bioelectronic interface in an animal model via in vivo polymerization of conjugated oligomers. *Bioactive Materials*. 2022/04/01/ 2022;10:107-116. doi:https://doi.org/10.1016/j.bioactmat.2021.08.025
101. Galeb HA, Wilkinson EL, Stowell AF, et al. Melanins as sustainable resources for advanced biotechnological applications. *Global challenges*. 2021;5(2):2000102.
102. Ovsianikov A, Mühleder S, Torgersen J, et al. Laser Photofabrication of Cell-Containing Hydrogel Constructs. *Langmuir*. 2014/04/08 2014;30(13):3787-3794. doi:10.1021/la402346z
103. Torgersen J, Ovsianikov A, Mironov V, et al. Photo-sensitive hydrogels for three-dimensional laser microfabrication in the presence of whole organisms. *Journal of biomedical optics*. 2012;17(10):105008.
104. Liu Y, Li J, Song S, et al. Morphing electronics enable neuromodulation in growing tissue. *Nature Biotechnology*. 2020/09/01 2020;38(9):1031-1036. doi:10.1038/s41587-020-0495-2
105. Hardy JG. Photoinitiating polymerisable composition. Google Patents; 2019.
106. Urciuolo A, Poli I, Brandolino L, et al. Intravital three-dimensional bioprinting. *Nature Biomedical Engineering*. 2020/09/01 2020;4(9):901-915. doi:10.1038/s41551-020-0568-z
107. Chen Y, Zhang J, Liu X, et al. Noninvasive in vivo 3D bioprinting. *Science Advances*. 6(23):eaba7406. doi:10.1126/sciadv.aba7406
108. Benedetto A, Bambade T, Au C, et al. New label-free automated survival assays reveal unexpected stress resistance patterns during C. elegans aging. https://doi.org/10.1111/acel.12998. *Aging Cell*. 2019/10/01 2019;18(5):e12998. doi:https://doi.org/10.1111/acel.12998
109. Coburn C, Allman E, Mahanti P, et al. Anthranilate fluorescence marks a calcium-propagated necrotic wave that promotes organismal death in C. elegans. *PLoS biology*. 2013;11(7):e1001613.
110. Olmedo M, Geibel M, Artal-Sanz M, Merrow M. A High-Throughput Method for the Analysis of Larval Developmental Phenotypes in Caenorhabditis elegans. *Genetics*. 2015;201(2):443-448. doi:10.1534/genetics.115.179242
111. Miller S, Selgelid MJ. Ethical and Philosophical Consideration of the Dual-use Dilemma in the Biological Sciences. *Science and Engineering Ethics*. 2007/12/01 2007;13(4):523-580. doi:10.1007/s11948-007-9043-4
112. Jarchum I. The ethics of neurotechnology. *Nature Biotechnology*. 2019/09/01 2019;37(9):993-996. doi:10.1038/s41587-019-0239-3
113. Laurie G. Novel Neurotechnologies: Intervening on the Brain. 2014;
114. Pfotenhauer SM, Frahm N, Winickoff D, Benrimoh D, Illes J, Marchant G. Mobilizing the private sector for responsible innovation in neurotechnology. *Nature Biotechnology*. 2021/06/01 2021;39(6):661-664. doi:10.1038/s41587-021-00947-y
115. Lawman S, Dong Y, Williams BM, et al. High resolution corneal and single pulse imaging with line field spectral domain optical coherence tomography. *Optics express*. 2016;24(11):12395-12405.
116. Dong Y, Lin H, Abolghasemi V, Gan L, Zeitler JA, Shen Y-C. Investigating Intra-Tablet Coating Uniformity With Spectral-Domain Optical Coherence Tomography. *Journal of Pharmaceutical Sciences*. 2017/02/01/ 2017;106(2):546-553. doi:https://doi.org/10.1016/j.xphs.2016.09.021
117. Lin H, Zhang Z, Markl D, Zeitler JA, Shen Y. A Review of the Applications of OCT for Analysing Pharmaceutical Film Coatings. *Applied Sciences*. 2018;8(12)doi:10.3390/app8122700

118. Zhang Z, Ikpatt U, Lawman S, et al. Sub-surface imaging of soiled cotton fabric using full-field optical coherence tomography. *Optics Express*. 2019/05/13 2019;27(10):13951-13964. doi:10.1364/OE.27.013951
119. Kuo ACM. Poly (dimethylsiloxane). *Polymer data handbook*. 1999:411-435.
120. Benitez DP, Jiang S, Wood J, et al. Knock-in models related to Alzheimer's disease: synaptic transmission, plaques and the role of microglia. *Molecular Neurodegeneration*. 2021/07/15 2021;16(1):47. doi:10.1186/s13024-021-00457-0
121. Stiernagle T, WormBook I. The C. elegans Research Community. *WormBook*. 2006:1551-8507.
122. Lima RT, Sousa D, Paiva AM, et al. Modulation of autophagy by a thioxanthone decreases the viability of melanoma cells. *Molecules*. 2016;21(10):1343.

Multiphoton fabrication was used produce 3D objects with integrated electronics (based on the conducting polymer, polypyrrole). The technique was used to print prototype integrated electronics in various substrates *in vitro* and in/on *C. elegans in vivo*. This approach potentially enables other researchers to produce integrated circuits designed for application-specific requirements *in vitro* and excitingly *in vivo*.

Keyword bioelectronics

S. J. Baldock, P. Kevin, G. R. Harper, R. Griffin, H. H. Genedy, M. J. Fong, Z. Zhao, Z. Zhang, Y. Shen, H. Lin, C. Au, J. R. Martin, M. D. Ashton, M. J. Haskew, B. Stewart, O. Efremova, R. N. Esfahani, H. Emsley, J. B. Appleby, D. Cheneler, D. M. Cummings, A. Benedetto*, J. G. Hardy*

Creating 3D objects with integrated electronics via multiphoton fabrication *in vitro* and *in vivo*